Biochemical and Biophysical Research Communications 462 (2015) 221–226

Contents lists available at ScienceDirect

Biochemical and Biophysical Research Communications

journal homepage: www.elsevier.com/locate/ybbrc

Molecular and topological membrane folding determinants of transient receptor potential vanilloid 2 channel

Pau Doñate-Macian [a, 1], Manuel Bañó-Polo [b, 1], Jose-Luis Vazquez-Ibar [a], Ismael Mingarro [b, **], Alex Perálvarez-Marín [a, *]

[a] Departament de Bioquímica i de Biologia Molecular, Unitat de Biofísica, Universitat Autònoma de Barcelona, 08193 Bellaterra, Spain
[b] Department of Biochemistry and Molecular Biology, ERI BioTecMed, University of Valencia, Dr. Moliner 50, 46100 Burjassot, Spain

ARTICLE INFO

Article history:
Received 22 April 2015
Available online 5 May 2015

Keywords:
Ion channels
TRP channels
Membrane protein trafficking
Membrane protein folding and biogenesis
Calcium signaling

ABSTRACT

Transient Receptor Potential (TRP) channels are related to adaptation to the environment and somatosensation. The transient receptor potential vanilloid (TRPV) subfamily includes six closely evolutionary related ion channels sharing the same domain organization and tetrameric arrangement in the membrane.

In this study we have characterized biochemically TRPV2 channel membrane protein folding and transmembrane (TM) architecture. Deleting the first N-terminal 74 residues preceding the ankyrin repeat domain (ARD) show a key role for this region in targeting the protein to the membrane. We have demonstrated the co-translational insertion of the membrane-embedded region of the TRPV2 and its disposition in biological membranes, identifying that TM1-TM4 and TM5-TM6 regions can assemble as independent folding domains. The ARD is not required for TM domain insertion in the membrane. The folding features observed for TRPV2 may be conserved and shared among other TRP channels outside the TRPV subfamily.

1. Introduction

Transient Receptor Potential (TRP) channels are polymodal cation channels with physiological key roles represented in six subfamilies in mammals [1]. The vanilloid subfamily in mammals consists of 6 members (TRPV1-6) with a very defined topology of two cytosolic domains flanking a membrane-embedded region. The TRPV1-4 subgroup has been defined as non-selective cation channels, whereas TRPV5-6 are calcium selective. The closest homologs are TRPV5 and TRPV6, sharing a 75% sequence identity [2]. The most studied member of the TRPV subfamily is TRPV1, the capsaicin receptor, which structure has been recently solved at high resolution. This structure showed a tetrameric arrangement of 6 transmembrane (TM) helices per monomer in TRPV1 with a topology and tetrameric arrangement similar to sodium channels [3], which is likely to be shared among the different TRPV members. The TRPV1-4 subgroup has a low sequence identity (TRPV1 and TRPV2 are the closest homologs with about 50% sequence identity), although evolutionary pressure patterns are similar [4].

Translocation of TRPV2 towards the plasma membrane has been observed in the presence of physical stimuli, growth factors or chemotactic peptides [5]. Recently, the possibility has arisen that TRPV2 functions as an intracellular or plasma membrane ion channel in a cell type/tissue dependent manner [6]. Thus it is key to define which TRPV2 domains are in charge for the sub-cellular localization and the proper folding of the channel.

Most membrane-embedded proteins are inserted and assembled in the ER membrane at sites termed translocons [7]. During this process, the translocon mediates the integration of TM sequences into the non-polar core of the membrane and delivers hydrophilic cytoplasmic and luminal domains to the appropriate

Abbreviations: ARD, ankyrin repeat domain; EGFP, enhanced green fluorescent protein; TM, transmembrane; TMD, transmembrane domain; TMHMM, TM hidden Markov model; TRP, transient receptor potential; TRPV, transient receptor potential vanilloid subfamily.

* Corresponding author. Centre d'Estudis en Biofísica/Unitat de Biofísica, Edifici M, Universitat Autònoma de Barcelona, 08193 Bellaterra, Barcelona, Spain. Fax: +34 935811907.
** Corresponding author. Department of Biochemistry and Molecular Biology/ERI BioTecMed, Dr. Moliner 50, University of Valencia, 46100 Burjassot, Spain. Fax: +34 963544635.
E-mail addresses: Ismael.Mingarro@uv.es (I. Mingarro), peralvarezmarin@gmail.com (A. Perálvarez-Marín).
[1] These authors contributed equally to this work.

http://dx.doi.org/10.1016/j.bbrc.2015.04.120
0006-291X/

compartments. Simultaneously, the nascent protein may undergo covalent modifications (e.g. *N*-glycosylation) and fold properly to eventually adopt its native state. *N*-glycosylation is cotranslationally performed in the lumen of the ER by the enzyme oligosaccharyltransferase, which is adjacent to the translocon [8]. TRPV2 has canonical *N*-glycosylation sites, $N_{571}N_{572}ST$, thus integration of the protein into ER-derived membranes can be monitored by *N*-glycosylation.

In this study we have applied a combination of biochemical approaches focusing on key molecular aspects of the TRPV2 channel related to membrane location, transmembrane architecture and folding. Some of the conclusions derived from this study can be relevant for the other members of the TRPV subfamily and other ion channels.

2. Materials and methods

2.1. Plasmids

cDNA sequences for rat TRPV2 were cloned into a pCDNA3 vector. The TRPV2 ORF was encoded in frame with an EGFP tag and an 8XHis-tag at the C-terminus. The N-terminus truncations for TRPV2 were obtained by classical PCR cassette reaction and ligated into pCDNA3 within NdeI and NotI sites.

2.2. Cell culture and transfection

HEK293 cells were cultured in Dulbecco's modified Eagle's medium (DMEM) supplemented with 10% FBS, 100 units/mL penicillin and 100 μg/mL streptomycin. Transfection was performed using polyethyleneimine (PEI, Polysciences, 23966). HEK293 cells overexpressing the transfected constructs were harvested 48 h after transfection and cells were lysed and membrane proteins solubilized for 15 min at 4 °C in detergent-containing buffer (50 mM Tris–HCL pH 7.4, 150 mM NaCl, 2 mM EDTA, 1% Triton, 5% glycerol, 1 mM benzamidine and EDTA-free protease inhibition cocktail, ROCHE 11873580001). The total fractions were centrifuged at 14000 g for 10 min. The supernatant was labeled as soluble (S) and the non-solubilized pellet was dissolved using a volume of buffer equal to the supernatant's volume and labeled as non-solubilized (P). EGFP-containing cell extracts could be visualized in an SDS-PAGE using a blue light box to monitor EGFP emission. Quantification of bands has been carried out using ImageJ gel analyzer tool [9].

2.3. MTT viability assay

24 h after transfecting HEK293T cells, cells were plated at 40,000 cells/well density in a 96 well plate. 48 h transfected cells were incubated with 3-(4,5-Dimethylthiazol-2-yl)-2,5-Diphenyltetrazolium Bromide (MTT) reagent (Invitrogen, M6494) for 3.5 h at 37 °C and the absorbance at 590 nm was measured with a FluoStar Optima microplate reader (BMG Labtech).

2.4. Biotinylation assay

Transfected HEK293 cells were washed with phosphate buffered saline (PBS) and incubated with sulfo-NHS biotin (0.5 mg/ml) for 30 min at 4 °C in an orbital shaker. After incubation cells were washed with PBS, quenched with a solution of 50 mM glycine and 50 mM ammonium chloride in PBS and washed with PBS. Cells were lysed in IP buffer pH = 7.4 (PBS, 1% Triton, 5% glycerol, 2.5 mM calcium chloride, 1 mM magnesium chloride, 5 mM EDTA, 5 mM EGTA, 10 mM sodium pyrophosphate, 50 mM sodium fluoride, 1 mM NaVO3, 1 mM benzamidine and EDTA-free protease inhibition cocktail, ROCHE). Cell extracts were incubated for 15 min at 4 °C and centrifuged at 14,000× *g* for 10 min. 500 μg of total protein from the cell extracts were incubated for 3 h at 4 °C with 50 μL neutravidin beads. Immunoprecipitated complexes were denatured with SDS-PAGE sample buffer (90 °C for 5 min), separated by SDS-PAGE and analyzed by immunoblotting. Scanned films were quantified using ImageJ gel analyzer tool [9]. For exocytosis inhibition, transfected HEK293 cells were treated with 50 μM Exo1 (SantaCruz, sc-200752) 2 h prior to biotinylation treatment. To allow the comparison of protein levels between the samples, all samples were loaded into the same gel.

2.5. Immunoblotting

Lysates and inmunoprecipitates were loaded into SDS-PAGE and transferred to a nitrocellulose membrane. Membranes were blocked in TBS-T with 5% (w/v) non-fat dry milk powder and incubated with primary anti His-Tag antibody from Developmental Studies Hybridoma Bank (DHSB mouse P5A11) at 1:1000 dilution and secondary antibody (Santa Cruz, anti mouse sc-2031) at 1:3000 dilution. Detection was carried out with Crescendo reagent (Millipore, WBLUR0100).

2.6. Microscopy and image analysis

Transfected cells on glass bottom microwell dishes (MATTEK) were in vivo visualized using a Leica TCS SP5 confocal microscope with a lens PL APO 40x/1.25–0.75. Cells were incubated 5 min with CellMask Deep Red Plasma Membrane (Life Technologies, C-10046) and HOESCH dyes (Life Technologies, H1399) before visualization. At least five fields were captured for each sample, yielding a total of $\geq$40 cells visualized.

2.7. Transmembrane topology experiments

TRPV2 truncated constructs were obtained by using forward primers that include the SP6 promotor sequence at the 5′ end and reverse primers at defined positions with an N-glycosylation C-terminal tag followed by tandem stop codons (Table S1) [10]. *In vitro* transcription and translation were performed as previously reported [11]. After membrane pelleting, samples were analyzed by SDS-PAGE, and gels were visualized on a Fuji FLA3000 phosphorimager using the ImageGauge software. The membrane insertion efficiency of a given truncated form was calculated as the quotient between the intensity of the singly glycosylated band divided by the summed intensities of the non-glycosylated and singly glycosylated bands.

2.8. TRPV2 modeling and docking into the TRPV2 EM map

The rat TRPV2 homology model was built using the Modeller [12] built-in in UCSF Chimera [13] using the rat TRPV1 coordinates (PDB code 3j5p). The membrane-embedded domain of TRPV2 was restrained to the topology experiments. TRPV2 homology model docking into the electron microscopy (EM) map of TRPV2 (code EMDB-5688, [14]) was carried out in UCSF Chimera. The TRPV2 EM map was flipped horizontally to show the same handedness of the TRPV1 structure.

3. Results and discussion

3.1. N-terminus of TRPV2 is involved in cell membrane localization

To characterize structural and physiological aspects related to the N-terminus of TRPV2 we studied two N-terminal truncations of

rat TRPV2 (rTRPV2); first, a deletion involving the 74 residues preceding the ARD (ΔN74-rTRPV2), and second, a truncation involving the entire ARD (ΔARD-rTRPV2), i.e. a rat TRPV2 protein variant with the first 336 residues deleted (Fig. 1A). Taking advantage of rTRPV2-EGFP fusions, we analyzed the protein expression levels by in-gel fluorescence of the full-length and truncated forms for rTRPV2 in HEK293T cells (Fig. 1B). Complete solubilization was not achieved using Triton X-100, but the full length and truncated forms were observed at similar levels in the non-solubilized (P) and the solubilized (S) fractions (Fig. 1B). Due to the heterologous expression of the different isoforms, we needed to verify that no observable differences arose from toxicity effects derived from protein overexpressions in HEK293T cells. The toxicity associated to the expression of GFP fused proteins was evaluated by means of an MTT assay, comparing to non-transfected cells, and to the EGFP alone (vector). No significant toxicity effects on HEK293T cells related to the presence of rat TRPV2 could be observed (Fig. 1C), as compared to another study showing cytotoxic effects in mouse TRPV2-transfected cells [15]. We also evaluated the cellular distribution of the full-length TRPV2 compared to the truncated forms. In Fig. 2A we provide an illustrative representation for the TRPV2 subcellular localization of the different constructs, all of them resulting in an internal-membrane rich TRPV2 localization. Image analysis of co-localization shows that the deletion of either the first 74 or 336 residues (ΔN74 or ΔARD constructs) of TRPV2 leads to a strong reduction of TRPV2 in the plasma membrane of HEK293T cells (Fig. 2A). To quantitate the localization of TRPV2 in the plasma membrane we performed a surface biotinylation assay [6,16]. TRPV2 was precipitated from biotinylated HEK293T cells (Fig. 2B) indicating that a fraction of TRPV2 is present in the plasma membrane of the transfected cells. The percentage of membrane-localized TRPV2 is significantly decreased either by the ΔN74 or ΔARD truncations (first 74 or 336 amino acids, respectively) (Fig. 2C). As a control, we inhibited TRPV2 targeting from the ER to the membrane by treating HEK293T transfected cells with an exocytosis inhibitor, 2-(4-Fluorobenzoylamino)-benzoic acid methyl ester (Exo1) (Fig. 2C), which induces a rapid collapse of the Golgi [17].

In sequence length, TRPV2 is the shortest within the TRPV1-4 subgroup (e.g. human sequences for TRPV1, TRPV2, TRPV3, and TRPV4 are 839, 764, 790, and 871 residues, respectively), displaying the shortest N-terminal region compared to TRPV1, TRPV3, and TRPV4. We observe that the first N-terminal 74 residues of TRPV2 play a role in the subcellular localization of the protein, such as targeting to the plasma membrane, since the deletion of this region leads to strong intracellular accumulation of the protein channel (Fig. 2).

3.2. Cotranslational insertion of TRPV2 membrane-embedded domain

To address that the N-terminus truncations do not yield intracellular accumulation of the channel due to improper packing/folding of the TRPV2 membrane-embedded domain we have performed further membrane protein topology studies.

TRPV2 lacking the first 336 residues and defining the membrane-embedded domain (residues 337–654) was translated *in vitro* in reticulocyte lysate in the presence of rough microsomes (RM). Most of this protein was glycosylated, which is detected by an increase in molecular mass of about 2.5 kDa (Fig. 3, lane 3). The TRPV2 membrane-embedded sequence contains an endogenous acceptor site for *N*-linked glycosylation: $N_{571}N_{572}ST$. No glycosylation was observed when a double mutant harbouring the consecutive Asn residues replaced by serines was translated in the presence of RMs (Fig. 3, lane 5). Therefore, the acceptor site

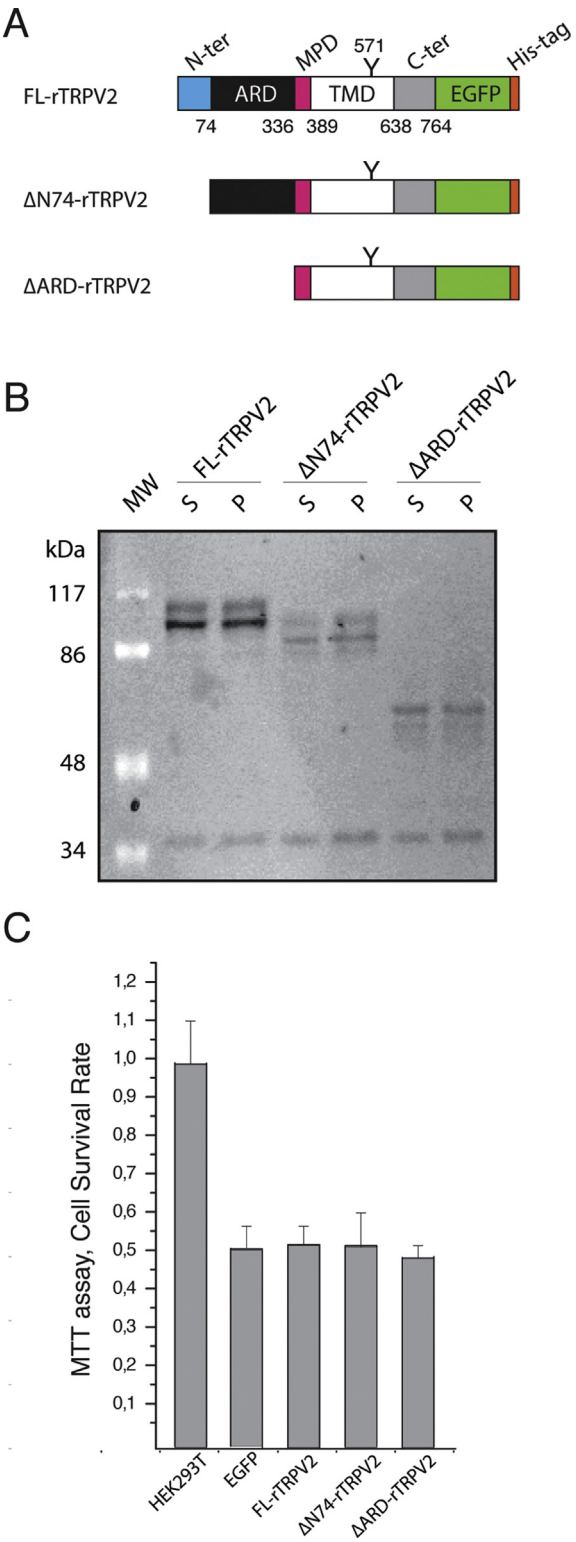

Fig. 1. Heterologous expression of TRPV2 N-terminal constructs. A. The domain organization of a TRPV2 monomer is displayed as a color-coded cartoon: N-terminus, blue; ARD, black; pre-TMD, pink; TMD, white; C-terminus, grey; EGFP, green; His-tag, orange. The *N*-glycosylation site is highlighted by a Y-shaped symbol. B. In-gel fluorescence indicating the expression of the truncations in HEK293T cells. TRPV2 wild type and truncations were extracted from membranes and present in the soluble fraction. C. MTT assay to determine the survival rate of HEK cells transfected with the defined rat TRPV2 truncations. (For interpretation of the references to color in this figure legend, the reader is referred to the web version of this article.)

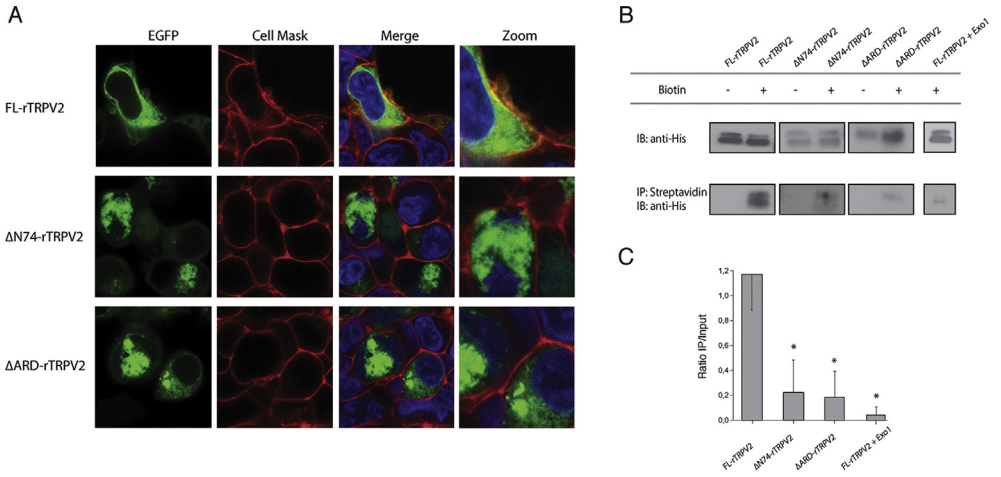

Fig. 2. TRPV2 cellular localization. A. Confocal imaging for HEK293T cells transfected with rat TRPV2 truncations. The left panel corresponds to the EGFP signal; the middle panel corresponds to the CellMask dye. The two right panels (merge) overlays the EGFP and CellMask channels also including the HOESCH channel to mark nuclei. B. Biotinylation assay for TRPV2 and the N-terminal truncations determining the amount of protein present in the plasma membrane. For each biotinylation experiment (N = 3), and for quantification purposes, samples were loaded in the same gel, and analyzed in the same film. C. Quantification of 3 independent biotinylation assays.

$N_{571}N_{572}ST$ is cotranslationally glycosylated *in vitro*, suggesting that the cytosolic N-terminus comprising the first 336 residues (ΔN74 and ΔARD constructs) is not required for membrane packing/folding of the protein.

3.3. Ordered membrane insertion of TRPV2 membrane-embedded domain

Next, we predicted the topology of TRPV2 membrane-embedded region using two commonly used prediction algorithms, i.e. the TM hidden Markov model (TMHMM) [18] and the experimentally based ΔG Predictor [19] methods to assess the segments with the higher probabilities to span biological membranes. As seen in Fig. 4A both methods roughly agree in their prediction outputs. Nevertheless, the membrane-buried segment of TM3 does not coincide in both predictions.

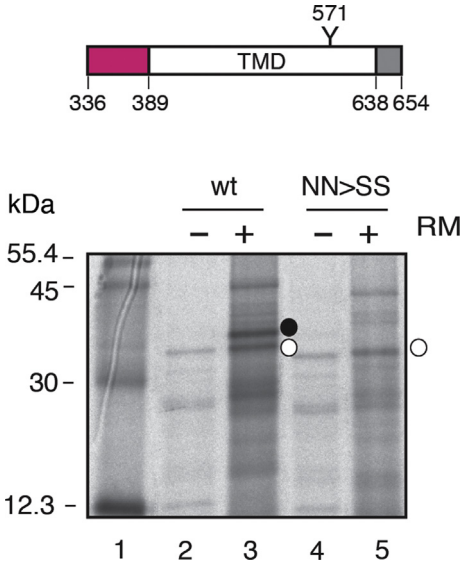

Fig. 3. TRPV2 is cotranslationally inserted into RMs and glycosylated at $N_{571}N_{572}ST$ acceptor site. Full-length TRPV2 membrane-embedded region and TRPV2-derived construct NN > SS containing the mutations Asn571Ser and Asn572Ser. Both constructs were translated *in vitro* in the presence of [^{35}S]Met/Cys and in the absence (−) and in the presence (+) of dog pancreas RMs. Bands of non-glycosylated proteins are indicated by a white dot and glycosylated proteins are indicated by a black dot. Molecular weight markers are shown on the left (lane 1).

Since *N*-linked glycosylation occurs in a compartment-specific manner, this modification can provide valuable topological information [20]. Thus, to experimentally map the membrane-embedded domain of the TRPV2, we used *N*-glycosylation as a topological reporter [21]. We prepared a series of protein truncates containing an added C-terminal glycosylation tag (NSTMGM) that has been proven to be efficiently modified in the *in vitro* translation system [10]. As shown in Fig. 4B, translation products containing residues 336–432 (truncated 96-mer polypeptides) of TRPV2, including the first predicted TM segment (TM1), were efficiently glycosylated in the presence of RMs (52 ± 4% of glycosylation), supporting the expected N-terminal cytoplasmic orientation for TM1. Truncated 134-mer polypeptides, which include residues 336–470 (Fig. 4A), were not glycosylated (6 ± 3% of glycosylation), indicating that the second predicted TM segment (TM2) efficiently integrates into the membrane (see Fig. 4B top for an illustrative scheme). The precise location of the third predicted TM segment was tested by translating a 159-residue truncation (residues 336–495). According to the TMHMM prediction, TM3 would span from residue 462 to residue 484, whilst according to the ΔG Predictor TM3 would end at residue 492. It has been previously reported that glycosylation occurs when the acceptor Asn is ~11–13 residues away from the membrane [22,23]. Therefore, since 159-mer polypeptides are not glycosylated (see Fig. 4B, lane 6), TM3 may extend up to Met492. To corroborate TM3 positioning, we added a previously used flexible amino acid linker [24] to extend the Asn glycosylation acceptor site farther away from the membrane ((159 + 10)-mer). Translation *in vitro* of this construct in the presence and in the absence of RMs (Fig. 4B, lanes 7 and 8) rendered glycosylated forms, placing the C-terminal end of the membrane-embedded TM3 segment around residue 492, in perfect agreement with the segment predicted by the ΔG Predictor (residues 471–492).

Furthermore, insertion of TM4 was analyzed by translating a 200-residue truncation (residues 336–536). The low level of glycosylation observed (26 ± 4%, Fig. 4B lane 10) indicates that the predicted fourth TM segment was significantly inserted. Truncated polypeptides encompassing residues 336–609, which include the native potential glycosylation site $N_{571}N_{572}ST$, were doubly

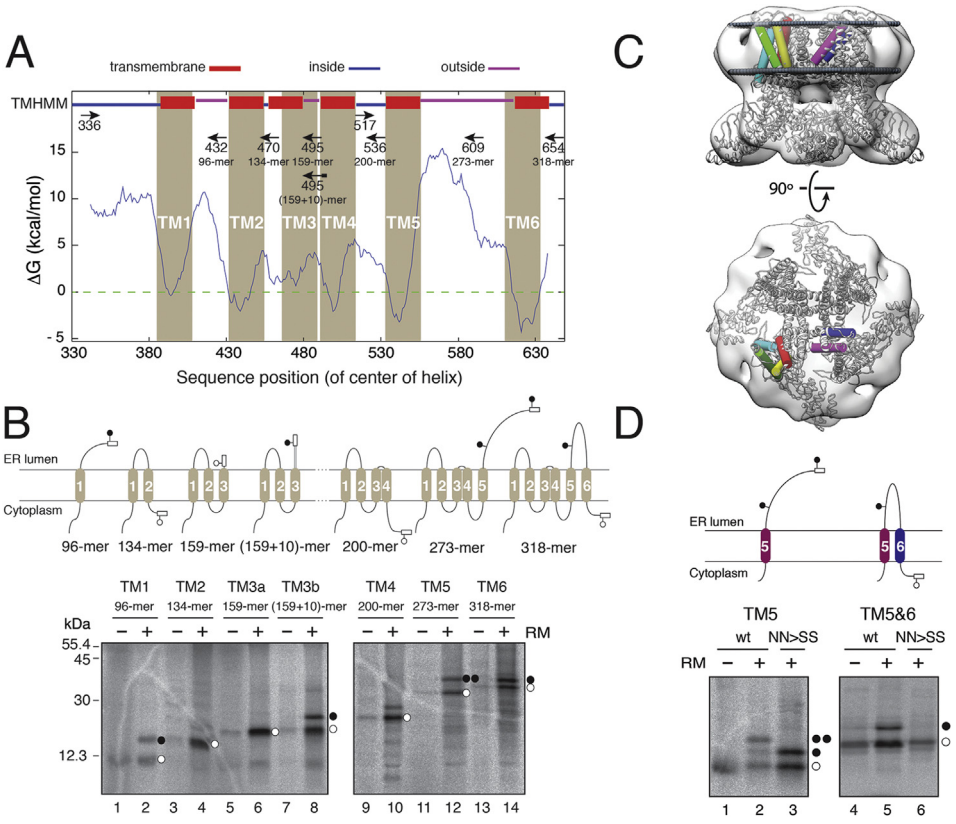

Fig. 4. TRPV2 TM segments are sequentially inserted into the ER membrane. A. Topology prediction for full-length TRPV2 membrane-embedded region using TMHMM [18] and the experimentally based ΔG Predictor [19] methods. In the TMHMM prediction method (top line), TM domains (red rectangles), cytoplasmic loops (blue lines) and luminal loops (pink lines) are indicated. In the ΔG Predictor, the ΔG graph (blue line) shows the predicted membrane-insertion efficiency along the sequence and the predicted TM domains are highlighted in brown. A set of oligonucleotides (arrows) was designed to generate TRPV2-truncated forms, which are indicated by the length of the truncated polypeptide (-mer) and the starting and ending residue in the TRPV2 sequence. B. *In vitro* expression and representative SDS-PAGE analysis of TRPV2 truncates. The presence of RMs and non-glycosylated and glycosylated polypeptides (empty and black dots, respectively) is indicated. Models of the membrane topology of truncated TRPV2 constructs are illustrated, in which a fused C-terminal *N*-glycosylation tag (rectangle) provides a simple readout for topology determination. C. Homology model of the tetrameric TRPV2 has been built using the membrane-embedded domain topology resulting from this study and docked into the TRPV2 EM map at 13.6 Å [14]. A monomer of the channel has been depicted using colored cylinders using the following color code: TM1, cyan; TM2, green; TM3, yellow; TM4, red; TM5, purple; TM6, blue. The spheres displayed in the top view indicate the limits of the lipid bilayer estimated using the OPM database [28]. D. *In vitro* translation of C-terminal-tagged mRNAs encoding TRPV2 and TRPV2-derived (NN > SS) constructs including TM5 (residues 517–609) and TM5-6 hairpin (residues 517–654) was performed in the presence (+) and absence (−) of membranes as indicated. Bands of non-glycosylated polypeptides are indicated by a white dot and singly- and doubly-glycosylated proteins are indicated by one and two black dots, respectively. (For interpretation of the references to colour in this figure legend, the reader is referred to the web version of this article.)

glycosylated, indicating that TM5 efficiently integrates into the membrane. Finally, the single glycosylation of 318-mer construct (residues 336–654) carrying the C-terminal glycosylation tag, combined with the absence of glycosylation in the mutated version (NN > SS) of TRPV2 membrane-embedded region (Figs. 3 and 4B), supports the presence of an inserted sixth TM segment.

3.4. Fitting of a homology model of TRPV2 into the TRPV1 solved structure

Next, we built a homology model of rat TRPV2 based on the recently solved structure of rat TRPV1 (PDB code 3j5p, [3]) using the ΔG Predictor [19] predicted TM segments and the present experimental results as constraints (represented by ribbons in Fig. 4C). The TRPV2 membrane-embedded domain sequence prediction satisfies the TM helix disposition of TRPV2 built on the coordinates of the TM1-TM6 of TRPV1 (Fig. 4C, coloured cylinders). In addition, we fitted the homology model of TRPV2 on the low resolution EM map of TRPV2 (code EMDB-5688, [14]) (not shown).

Both the TRPV2 model and the 3D structure of TRPV1 show a large spatial gap between the TM1-4 and the TM5-6 segments due to a relatively long membrane interface domain between TM4 and TM5. This fact suggested the possibility of TM1-4 and TM5-6 acting as independent folding/assembly subunits.

3.5. Membrane insertion of TM5-TM6 hairpin

TRPV2 channel functions as a tetramer. As shown in Fig. 4C, in each monomer TM5 and TM6 seem to cluster away from the rest of the membrane-embedded domain (TM1-4) as an α-helical hairpin. This simple structural motif is thought to occur relatively frequently in integral membrane proteins and may serve as an important structural and/or functional element [25]. In the TRPV1 case, this helical hairpin has been implicated in the formation of the central ion-conducting pore of the tetramer [3]. To explore the possibility that TRPV2 TM5 and TM6 region could integrate into the membrane as an independent folding motif, we translated from Arg517 to Glu609 (Fig. 4D), a region that includes the extra-membranous loop connecting TM4 to TM5, the fifth TM segment and the native glycosylation site $N_{571}N_{572}ST$. As shown in Fig. 4D (lanes 1–3), doubly glycosylated forms were observed, suggesting that TM5 isolated from the rest of the membrane-embedded region is able to direct its integration into the ER membrane through the translocon. Furthermore, translation of truncated C-terminal

reporter tag fusions encompassing from Arg517 to Asp654, which extended the polypeptide to include TM6, show singly glycosylated forms, suggesting α-helical hairpin insertion (Fig. 4D, lane 5). Notably, single glycosylation and no glycosylation were observed when the native glycosylation acceptor site was mutated in these two constructs (Fig. 4D, lanes 3 and 6). Combined, these results support the independent α-helical hairpin motif integration into biological membranes.

Taking into account our experimental topological analysis, together with TRPVs evolutionary information [4] and the recent TRPV1 and TRPV2 structures [3,14], it is evident that the membrane-embedded domain of the TRPV1-4 shares a common membrane disposition. Interestingly, the insertion into the bilayer of TRPV channels is cotranslational and does not require the cytosolic N-terminal region (first 74 residues and the ARD), since our translation/insertion experiments were carried out in the absence of this domain. We have also identified that the TM1-TM4 and the TM5-TM6 regions of TRPV2 are capable of assembling separately in the membrane, acting as independent folding units. Thus, an independent folding of the TM1-TM4 and TM5-TM6 can be assumed for TRPV1-4 channels, and it cannot be ruled out for the equivalent region of other ion channels with similar topology such as potassium and/or sodium channels [26,27].

Conflict of interest

None declared.

Acknowledgments

The cDNA sample for rat TRPV2 was kindly provided by Prof. Rachelle Gaudet. The authors acknowledge the skillful assistance of Elodia Serrano, the funding from Spanish Government (MICINN-SAF2010-21385 to A.P.-M. and BFU2012-39482 to I.M.), a Marie Curie International Outgoing Fellowship within the 7th European Community Framework Programme (PIOF-GA-2009-237120 to A.P.-M.), the Generalitat de Catalunya research program (AGAUR, 2014-SGR-1628 to A.P.-M.) and the Generalitat Valenciana (PROMETEOII/2014/061 and ACOMP/2014/245 to I.M.). P.D.-M. is a recipient of an FI fellowship from Generalitat de Catalunya (FI–2013FIB00251); M.B.-P. was the recipient of an FPU fellowship from the Spanish Ministry of Education. A.P.-M. is a recipient of the Universitat Autònoma de Barcelona-Programa Banco de Santander Fellowship.

Appendix A. Supplementary data

Supplementary data related to this article can be found at http://dx.doi.org/10.1016/j.bbrc.2015.04.120.

Transparency document

Transparency document related to this article can be found online at http://dx.doi.org/10.1016/j.bbrc.2015.04.120.

References

[1] B. Nilius, G. Owsianik, The transient receptor potential family of ion channels, Genome Biol. 12 (2011) 218.
[2] M.J. Gunthorpe, C.D. Benham, A. Randall, J.B. Davis, The diversity in the vanilloid (TRPV) receptor family of ion channels, Trends Pharmacol. Sci. 23 (2002) 183–191, http://dx.doi.org/10.1016/S0165-6147(02)01999-5.
[3] M. Liao, E. Cao, D. Julius, Y. Cheng, Structure of the TRPV1 ion channel determined by electron cryo-microscopy, Nature 504 (2013) 107–112.
[4] P. Doñate-Macián, A. Perálvarez-Marín, Dissecting domain-specific evolutionary pressure profiles of transient receptor potential vanilloid subfamily members 1 to 4, PLoS One 9 (2014) e110715, http://dx.doi.org/10.1371/journal.pone.0110715.
[5] A. Perálvarez-Marín, P. Doñate-Macian, R. Gaudet, What do we know about the transient receptor potential vanilloid 2 (TRPV2) ion channel? FEBS J. 280 (2013) 5471–5487, http://dx.doi.org/10.1111/febs.12302.
[6] M.R. Cohen, K.W. Huynh, D. Cawley, V.Y. Moiseenkova-Bell, Understanding the cellular function of TRPV2 channel through generation of specific monoclonal antibodies, PLoS One 8 (2013) e85392, http://dx.doi.org/10.1371/journal.pone.0085392.
[7] L. Martínez-Gil, A. Saurí, M.A. Marti-Renom, I. Mingarro, Membrane protein integration into the endoplasmic reticulum, FEBS J. (2011) 3846–3858, http://dx.doi.org/10.1111/j.1742-4658.2011.08185.x.
[8] I. Nilsson, D.J. Kelleher, Y. Miao, Y. Shao, G. Kreibich, R. Gilmore, et al., Photocross-linking of nascent chains to the STT3 subunit of the oligosaccharyltransferase complex, J. Cell Biol. 161 (2003) 715–725, http://dx.doi.org/10.1083/jcb.200301043.
[9] W.S. Rasband, ImageJ, U. S. Natl. Institutes Heal, Bethesda, Maryland, USA, 2012, pp. 1997–2012. http//imagej.nih.gov/ij/.
[10] M. Bañó-Polo, F. Baldin, S. Tamborero, M.A. Marti-Renom, I. Mingarro, N-glycosylation efficiency is determined by the distance to the C-terminus and the amino acid preceding an Asn-Ser-Thr sequon, Protein Sci. 20 (2011) 179–186, http://dx.doi.org/10.1002/pro.551.
[11] A. Saurí, S. Tamborero, L. Martínez-Gil, A.E. Johnson, I. Mingarro, Viral membrane protein topology is dictated by multiple determinants in its sequence, J. Mol. Biol. 387 (2009) 113–128, http://dx.doi.org/10.1016/j.jmb.2009.01.063.
[12] A. Fiser, A. Sali, Modeller: generation and refinement of homology-based protein structure models, Methods Enzymol. 374 (2003) 461–491.
[13] E.F. Pettersen, T.D. Goddard, C.C. Huang, G.S. Couch, D.M. Greenblatt, E.C. Meng, et al., UCSF Chimera–a visualization system for exploratory research and analysis, J. Comput. Chem. 25 (2004) 1605–1612, http://dx.doi.org/10.1002/jcc.20084.
[14] K.W. Huynh, M.R. Cohen, S. Chakrapani, H.A. Holdaway, P.L. Stewart, V.Y. Moiseenkova-Bell, Structural insight into the assembly of TRPV channels, Structure 22 (2014) 260–268, http://dx.doi.org/10.1016/j.str.2013.11.008.
[15] A. Penna, V. Juvin, J. Chemin, V. Compan, M. Monet, F.-A. Rassendren, PI3-kinase promotes TRPV2 activity independently of channel translocation to the plasma membrane, Cell Calcium 39 (2006) 495–507.
[16] C. Morenilla-Palao, R. Planells-Cases, N. García-Sanz, A. Ferrer-Montiel, Regulated exocytosis contributes to protein kinase C potentiation of vanilloid receptor activity, J. Biol. Chem. 279 (2004) 25665–25672.
[17] Y. Feng, S. Yu, T.K.R. Lasell, A.P. Jadhav, E. Macia, P. Chardin, et al., Exo1: a new chemical inhibitor of the exocytic pathway, Proc. Natl. Acad. Sci. U. S. A. 100 (2003) 6469–6474, http://dx.doi.org/10.1073/pnas.0631766100.
[18] A. Krogh, B. Larsson, G. von Heijne, E.L. Sonnhammer, Predicting transmembrane protein topology with a hidden Markov model: application to complete genomes, J. Mol. Biol. 305 (2001) 567–580, http://dx.doi.org/10.1006/jmbi.2000.4315.
[19] T. Hessa, N.M. Meindl-Beinker, A. Bernsel, H. Kim, Y. Sato, M. Lerch-Bader, et al., Molecular code for transmembrane-helix recognition by the Sec61 translocon, Nature 450 (2007) 1026–1030.
[20] L. Martínez-Gil, A.E. Johnson, I. Mingarro, Membrane insertion and biogenesis of the turnip crinkle virus p9 movement protein, J. Virol. 84 (2010) 5520–5527, http://dx.doi.org/10.1128/JVI.00125-10.
[21] I. Nilsson, G. von Heijne, Fine-tuning the topology of a polytopic membrane protein: role of positively and negatively charged amino acids, Cell 62 (1990) 1135–1141, http://dx.doi.org/10.1016/0092-8674(90)90390-Z.
[22] I. Nilsson, G. Von Heijne, Determination of the distance between the oligosaccharyltransferase active site and the endoplasmic reticulum membrane, J. Biol. Chem. 268 (1993) 5798–5801.
[23] M. Orzáez, J. Salgado, A. Giménez-Giner, E. Pérez-Payá, I. Mingarro, Influence of proline residues in transmembrane helix packing, J. Mol. Biol. 335 (2004) 631–640, http://dx.doi.org/10.1016/j.jmb.2003.10.062.
[24] S. Tamborero, M. Vilar, L. Martínez-Gil, A.E. Johnson, I. Mingarro, Membrane insertion and topology of the translocating chain-associating membrane protein (TRAM), J. Mol. Biol. 406 (2011) 571–582, http://dx.doi.org/10.1016/j.jmb.2011.01.009.
[25] M. Bañó-Polo, L. Martínez-Gil, B. Wallner, J.L. Nieva, A. Elofsson, I. Mingarro, Charge pair interactions in transmembrane helices and turn propensity of the connecting sequence promote helical hairpin insertion, J. Mol. Biol. 425 (2013) 830–840, http://dx.doi.org/10.1016/j.jmb.2012.12.001.
[26] X. Tao, J.L. Avalos, J. Chen, R. MacKinnon, Crystal structure of the eukaryotic strong inward-rectifier K+ channel Kir2.2 at 3.1 A resolution, Science 326 (2009) 1668–1674, http://dx.doi.org/10.1126/science.1180310.
[27] J. Payandeh, T. Scheuer, N. Zheng, W.A. Catterall, The crystal structure of a voltage-gated sodium channel, Nature 475 (2011) 353–358, http://dx.doi.org/10.1038/nature10238.
[28] M.A. Lomize, A.L. Lomize, I.D. Pogozheva, H.I. Mosberg, OPM: orientations of proteins in membranes database, Bioinformatics 22 (2006) 623–625, http://dx.doi.org/10.1093/bioinformatics/btk023.